ACCUMULATION DISTRIBUTION IN TERRE ADÉLIE, ANTARCTICA: EFFECT OF METEOROLOGICAL PARAMETERS

By P. PETTRE,

(Centre National de Recherche Meteorologiques, 31057 Toulouse Cedex, France)

J.F. PINGLOT, M. POURCHET, *and* L. REYNAUD

(Laboratoire de Glaciologie et Géophysique de l'Environnement, 38402 Saint-Martin-d'Hères Cedex, France)

ABSTRACT. Along the 1040 km extending from Cape Prud'homme (lat. 66°41′ S., long. 139°55′ E.), near Dumont d'Urville station, to Dome C (lat. 74°39′ S., long. 124°10′ E.), the variations in annual accumulation can be analysed by a division of the entire data set into three sub-sets depending on the types of measurements and the character of the spatial distribution. Along the first 33 km, from the coast to stake E40, annual measurements show considerable inter-annual variability, 52% of which can be explained by the spatio-temporal homogeneity of the balance distribution. However, we obtain a better result (64%) for the fluctuation homogeneity standardized using the standard deviation. This means that there is a strong space–time distribution structure, characterized by an equal variation of the balance around the mean value specific to each location. This is so in spite of the existence of considerable surface roughness (sastrugi), the influence of which should be reduced by averaging values around each stake. From stake E40 to stake R60, a distance of 170 km, the almost periodic oscillations in the accumulation with a wavelength close to 40 km can be explained by the formation of a gravity-inertia wave, disturbing the geostrophic equilibrium, occurring at the break in slope 200 km from the coast. The very low values of accumulation for stakes D55 and D58S show that the oscillations were almost stationary during the study period (about 25 years). Finally, along the 840 km from stake R60 to Dome C we can observe a decrease in accumulation resulting from the decrease in mean temperature.

RÉSUMÉ. *La distribution d'accumulation en Terre Adélie, Antarctique: effet de paramètres météorologiques.* Sur les 1040 km de Cap Prud'homme (66°41′ S., 139°55′ E.) situé à proximité immédiate de la station Dumont d'Urville à Dôme C (74°39′ S., 124°10′ E.) les variations de l'accumulation annuelle peuvent être analysées en partitionant l'ensemble des données en trois sous-ensembles en fonction des types de mesures et des caractères de distribution spatiale. Sur les 33 premiers km, de la côte à la balise E40, les mesures recueillies chaque année montrent une grande variabilité interannuelle dont une partie (52%) peuvent être expliquée par l'homogénéité de distribution du bilan. Cependant on obtient un meilleur score (64%) pour l'homogénéité de la fluctuation normée par l'écart type. C'est-à-dire qu'il existe une forte structure de répartition spatio-temporelle caractérisée par une variation identique du bilan autour de d'une important rugosité de surface (sastrugi), dont il la moyenne propre à chaque site. Ceci malgré l'existence

conviendrait de réduire l'influence en moyennant les mesures autour de chaque balise. De E40 à R60, sur 170 km, les oscillations quasi périodiques de l'accumulation avec une longueur d'onde voisine de 40 km peuvent s'expliquer par la formation d'une onde de gravité inertie perturbant l'équilibre géotropique prenant son origine à la rupture de pente vers 200 km de la côte. Les très faibles valeurs de l'accumulation pour les stations D55 et D58S indiquent que ces oscillations sont sensiblement stationnaires durant la période étudiée (25 ans environ). Enfin sur les 840 km de R60 à Dôme C on peut observer la décroissance de l'accumulation entraînée par la diminution des températures moyennes.

ZUSAMMENFASSUNG. *Verteilung des Schneeauftrages in Terre Adélie, Antarktika: Einfluss der meteorologischen Parameter.* Entlang des 1040 km langen Profils von Cape Prud'homme (66°41′ südl. Br., 139°55′ östl. L.) nahe der Station Dumont d'Urville zum Dome C (74°39′ südl. Br., 124°10′ östl. L.) können die Schwankungen der jährlichen Akkumulation durch Unterteilung des gesamten Datensatzes in drei Teilsätze in Abhängigkeit von den Messverfahren und vom Charakter der räumlichen Verteilung analysiert werden. Längs der ersten 33 km, von der Küste bis Pegel E40, zeigen die jährlichen Messungen eine beträchtliche Schwankungsbreite während des Jahres; 52% davon können mit der raum-zeitlichen Homogenität der Bilanzverteilung erklärt werden. Ein besseres Ergebnis (64%) für die standardisierte Schwankungshomogenität lässt sich jedoch gewinnen, wenn man die Standardabweichungen heranzieht. Das bedeutet, dass eine starke raum-zeitliche Verteilungs-struktur vorliegt, die sich durch eine gleichmässige Schwankung der Bilanz um den für jede Stelle spezifischen Mittelwert charakterisieren lässt. Dies gilt trotz einer erheblichen Oberflächenrauhigkeit (Sastrugi), deren Einfluss sich durch Mittelung der Werte im Umfeld jedes Pegels verringern sollte. Von Pegel E40 bis Pegel R60, auf eine Strecke von 170 km, können die nahezu periodischen Oszillationen in der Akkumulation mit einer Wellenlänge bei 40 km durch die Bildung von Schwerkraft-Trägheits-Wellen erklärt werden, die das geostrophische Gleichgewicht stören, das am Gefällsbruch 200 km von der Küste auftritt. Die sehr niedrigen Akkumulationswerte für die Pegel D55 und D58S zeigen, dass die Oszillationen während der Untersuch-ungsperiode (25 Jahre) nahezu stationär waren. Längs der 850 km von Pegel R60 bis Dome C schliesslich ist eine Abnahme der Akkumulation infolge der Abnahme der Mitteltemperatur zu beobachten.

INTRODUCTION

Snow accumulation at a fixed point is the result of the re-distribution and modification of fallen precipitation by various processes: wind and relief effects, thinning of the layers due to ice flow, melting, sublimation, etc.

For the Antarctic ice sheet, only the re-distribution induced by wind and relief plays an important part at the

surface. This phenomenon can sometimes cause major accumulation differences for stations only a few kilometers apart. When a fixed-point measurement is not the aim, this effect can be minimized by taking a representative sample with greater spatial coverage. The range often used for such smoothing is in the order of 50 km (Young and others, 1982). For the Terre Adélie area, where many measurements are available, each one covering the last two or three

decades, we have established a simple mathematical relationship which gives a good estimate of accumulation and which accounts for the spatial oscillations observed, starting at the break-in-slope with the Antarctic plateau. These oscillations could be the result of a meteorological phenomenon which is discussed in detail.

Time-scales for meteorology and glaciology are very much different: a few hours in the first case, several months in the latter. These two disciplines are difficult to compare and the assumptions made are therefore often difficult to check. However, we have confidence in our findings for Antarctica, because of its geophysical uniformity (proximity to the South Pole, permanent snow cover over the entire surface, less disturbed relief, etc.).

MEASUREMENTS AND SAMPLING TRAVERSES

Between January 1971 and January 1983, during several measurement and sampling traverses, the accumulation along the Dumont d'Urville–Dome C axis (Fig. 1) was determined at many stations in a stake network and also by ice-core analysis based on the radioactive reference levels due to atmospheric nuclear tests.
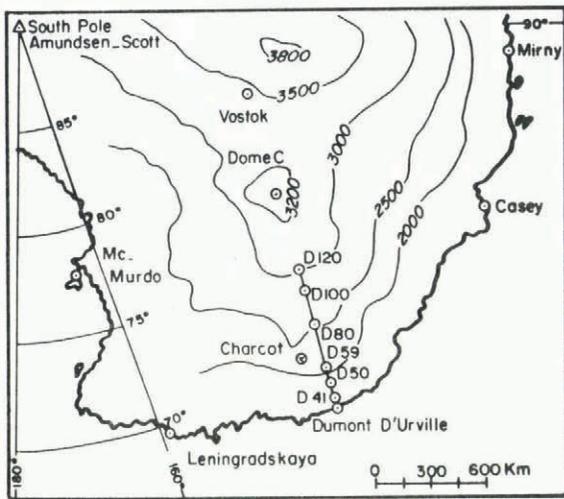

Fig. 1. Map of Antarctica showing the Terre Adélie area and the sampling traverse.

Between the coast and stake E40, located 33 km inland, 40 stakes were planted in January 1971. These stakes were measured every austral summer.

Beyond stake E40, the stake spacing is about 10 km. Moreover, for 31 stations between the coast and stake R80 (located 430 km inland), very accurate snow sampling has been conducted (generally more than six samples per year) for the measurement of total beta-radioactivity.

These measurements give the depths corresponding to the radioactive reference levels of January 1955 (Picciotto and Wilgain, 1963) and January 1965 (Crozaz, 1969) which have been widely used for dating snow layers in Antarctica (Picciotto and others, 1964; Lambert and others, 1977; Pourchet and others, 1983).

Between R80 and Dome C, accumulation is only known at two stations (D100 and D120). For Dome C, it corresponds to the mean value of 22 ice cores sampled over a few kilometers. Some of these results have already been published (Lorius and others, 1970; Lambert and others, 1977; Petit and others, 1982; Pourchet and others, 1983) and complementary profiles available are given here (Fig. 2a and b).

In parallel with accumulation measurements, the 10 m depth temperature of the snow was determined for about 30 stations. The measurements were made in ice-core holes during several traverses with thermistors pre-calibred over the relevant range. Their accuracy is about ±0.5°C.

Station elevations were initially measured by a barometric survey using a 10 km spacing (1971–72 traverse).

During this survey, pressures between two successive stations were measured simultaneously. During two other traverses (austral summers of 1980–81 and 1982–83) a Doppler-effect survey, between the coast and station R80, allowed us to determine accurately the elevation of 15 stations. For station R80, the difference between the two methods was 92 m.

These 15 stations also allowed us to calibrate a precise barometric survey (every 1 km) made during the 1982–83 traverse. Distance measurements were done for all the Doppler-effect located stations (accuracy within a few meters) with vehicle odometers.

The maximum spacing between two successive Doppler-effect located points was 50 km and the distance accuracy of intermediate points (measured by vehicle odometers) was about 1 km.

Between the coast and station E40, snow accumulation has been converted to water equivalent using a mean densification curve (Fig. 3). It results from the compilation of many density profiles available for this area. For the relevant depths, a good estimate of this density is given by the relationship:

$$D = -3.73 \times 10^{-4} z^2 + 0.01427z + 0.430$$

where D (Mg m^{-3}) represents mean density between the surface and depth z (expressed in meters).

Assuming that the bottom of each stake is firmly fixed relative to the snow layer in which it lies, the mean annual accumulation (A) is given by the relationship:

$$A = \frac{z_2 D_2 - z_1 D_1}{t_2 - t_1}$$

where z_2 and z_1 represent snow cover at the stake at times t_2 and t_1, and D_2 and D_1 are the mean densities between the surface and depths z_2 and z_1.

The mean annual accumulation between 1971 and 1983 was determined by this method for each stake (Table I).

Beyond station E40, the snow depth–water equivalent conversion was done using the densification curve of the nearest measured station, which was never further away than 30 km.

## INTERPRETATION OF THE ACCUMULATION MEASUREMENTS

Between the coast and stake E40

Along these first 33 km, a set of annual accumulation values measured at 40 stakes is available for the period 1971 to 1983 (Table I). The mean values of the annual balances are plotted in Figure 4 as a function of the distance to the coast, together with the mean surface slope between successive stakes. Note that each irregularity in the topography shows a corresponding major change on the balance curve, mainly involving a deficit up-stream of the break in slope and an excess just down-stream. But the main characteristic of this set of balance values is the great inter-annual variability, in the order of 70% of the mean. This value is slightly lower than that deduced from accumulation variations between the two decades 1955–65 and 1965–75 for a large part of Antarctica (Pourchet and others, 1983).

The question that immediately arises when confronted by a set of data affected by such high variability is whether these variations are randomly distributed or whether they in fact express a spatio-temporal distribution mode. This is important in a set of measurements in order to distinguish what is characteristic of the particular location from what may be a feature of the year; for example, to take into account several sets of measurements made at several stations in Antarctica when making a comparison.

For this purpose, we tested two mass-balance distribution models using the values in Table I, only retaining complete annual series, i.e. 16 stakes over a 10 year period (D05, 05 bis, 07, 08, 09, 10, 11, 15, 19, 21, 22, 23, 27, 36, and 37).

The first simple model tested was the one proposed by Lliboutry (1974), which assumes an equal inter-annual

487

a
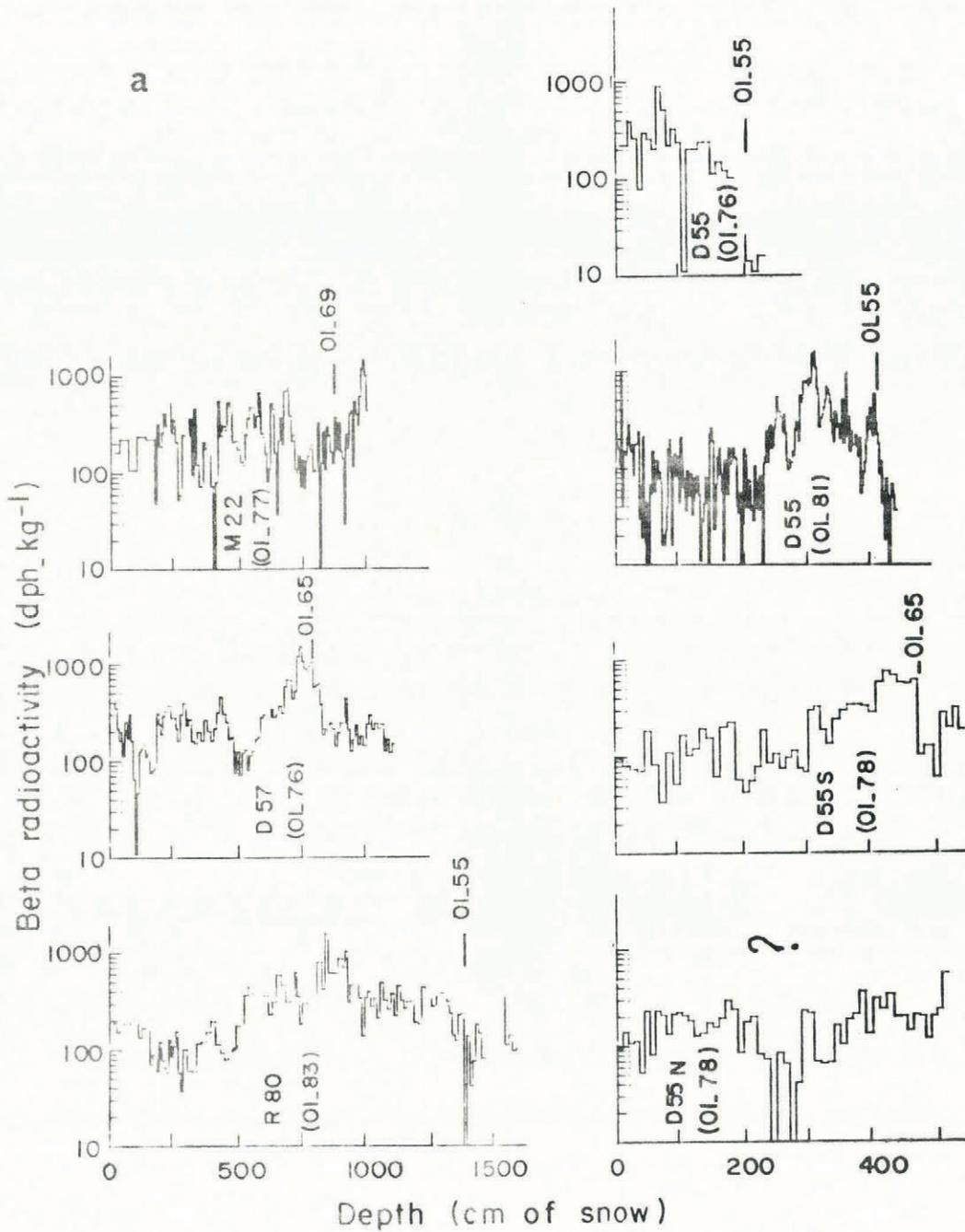
variation around the mean value of the balance for the stations. If b_{jt} is the balance measured at site j for year t, it may be broken down into three terms:

$$b_{jt} = \alpha_j + \beta_t + \epsilon_{jt}$$

where α_j is the mean value characteristic of site j, independent of time with

$$\alpha_j = \sum_{t=1}^{T} b_{jt} .$$

β_t is the centred variation of the balance

$$\left[\sum_{1}^{T} \beta_t = 0 \right],$$

which does not depend upon the site and is identical for all

the stakes, and ϵ_{jt} is a centred random residual, the standard deviation of which expresses the adequacy of the model with respect to reality. In practice, in order to test this model on real values by variance analysis, a table of centred values $b_{jt} - \alpha_j$, which are the terms of the expression $\beta_t + \epsilon_{jt}$, was deduced from the table of b_{jt} (J stakes and T years), for each of T years; the value of β_t is given by

$$\frac{1}{J} \sum_{J} (b_{jt} - \alpha_j)$$

and the real values for each stake are different by ϵ_{jt}.

The overall variance of the sample

$$S_t^2 = \sum_{t=1}^{T} \sum_{J=1}^{J} (b_{jt} - \alpha_j)^2$$

is the sum of the variance explained by an identical β_t each year at the J sites:
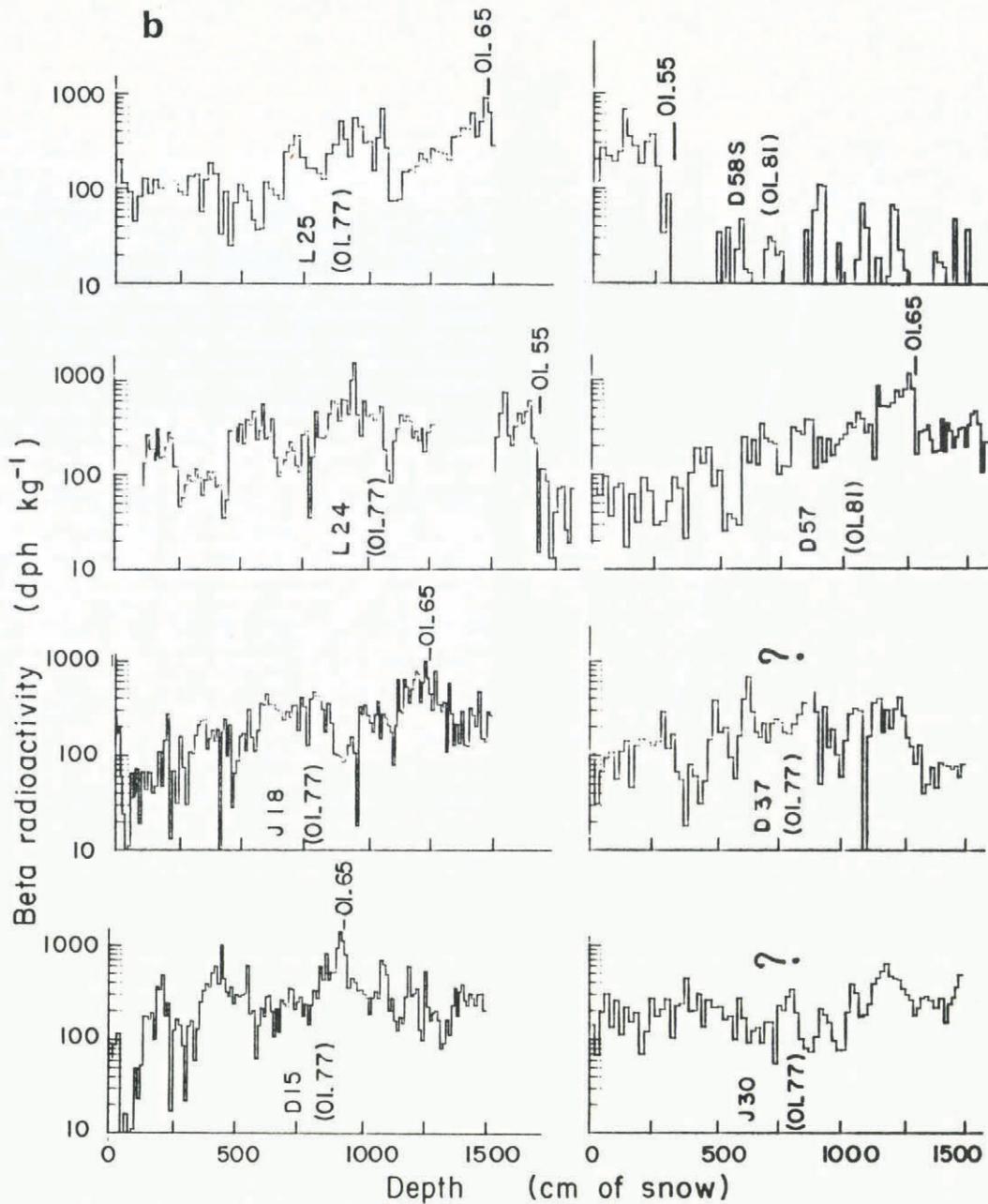
Fig. 2a and b. β radioactivity (in dph per kg of ice) versus depth (in cm of snow) along the Dumont d'Urville–R80 axis. For each station, the β levels used and the date of sampling ( ) are indicated.

$$S_e^2 = J \sum_1^T \beta_t^2$$

and the residual variance

$$S_r^2 = \sum_{t=1}^T \sum_{J=1}^J \epsilon_{jt}^2$$

$$S_t^2 = S_e^2 + S_r^2.$$

The degree of explanation $\tau = S_e^2/S_t^2$ is 0.52, indicating that the linear model of balance variation takes into account 52% of the total variance of the sample.

The remaining 48% unexplained by this model is expressed by a residual standard deviation of 19 cm of water equivalent, i.e. about 40 cm of snow. Note that this corresponds to the mean height of the sastrugi observed in the area. This shows that it would be worthwhile to add a network of bamboos around each stake in order to obtain a mean value of the accumulation over a few square meters which would be more representative of the site than the single-point value.

In fact, the incomplete values determined at four bamboo networks available for one axis and the year 1972 alone (Table II), although insufficient to lead to significant numerical results, confirm the importance which should be attached to micro-relief.

Note also that these observations are similar to those already formulated for Dome C station (lat. 74°39′S., long. 124°10′E.) where the surface micro-relief is responsible, at a fixed-point sample, for a background value of the same order of magnitude as the annual accumulation: $\sigma = 2.6$ g cm^{-2} year^{-1} for an accumulation of 3.6 g cm^{-2} year^{-1} (Petit and others, 1982).

However, we find that the linear model gives only a rough approximation, since it is based on identical standard deviations along the profile, while the table of measurements indicates that they are highly variable. A second
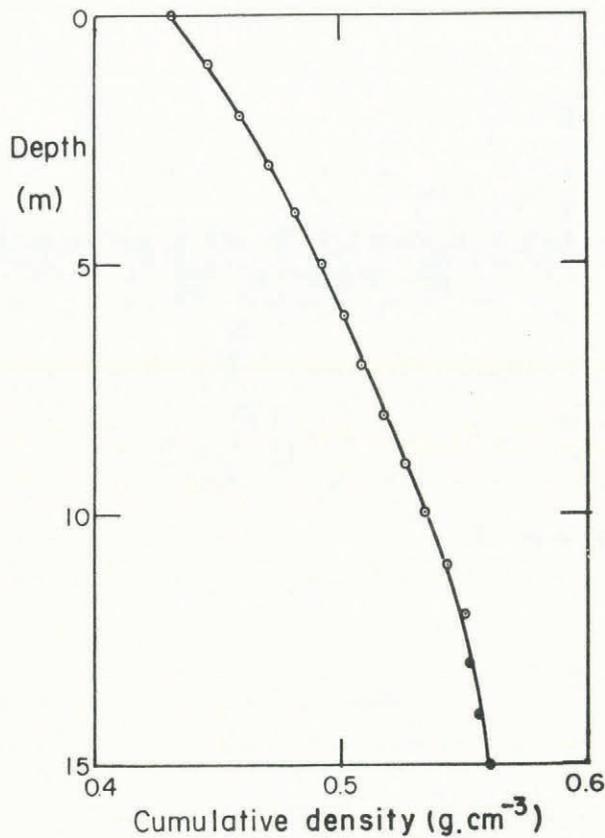
489

Depth (m)

Cumulative density (g.cm^{-3})

Fig. 3. Mean cumulative density curve between the coast and station E40. The cumulative density for the depth z is the density between the surface and depth z.

variance analysis can be conducted by comparing the variations of β_l for a site reduced by the standard deviation, in order to analyse the relative variations.

This is the basis of principal component analysis, which compares reduced centred fluctuations. The results are given in Figure 5 which shows a common factor responsible for 64% of the variance and a second factor accounting for 10% of the variance, with 26% distributed on the other axes.

Axis 1 is interpreted as the consequence of the variation of homogeneity of the reduced centred balance, while axis 2 shows another trend differentiating the values in an apparently geographic manner, from the coast to the interior; this is somewhat unclear and opposite to other balance distributions such as those found in alpine-type mountain ranges (Reynaud and others, 1984). Finally, no known structure is apparent for the 26% of the variance explained on the other axes.

This is, however, not surprising taking into account the conditions of snow redistribution on the surface by wind which forms sastrugi. Under these conditions, it can be said that the spatio-temporal distribution homogeneity is certainly even more marked than found, and that far better results could be obtained if we were able to eliminate the background noise induced by the sastrugi. Using both radioactivity measurements and stake values, we also computed the mean value of accumulation for all the stations in this area and for the widest time period available (Table III). In each case, we mention the methods used as well as the relevant time period and the number of years represented. In some cases, our observations are discontinuous and as a result the number of years represented may be less than the time period of observation. For each accumulation value, we calculated an uncertainty $\sigma = s/(n-1)^{\frac{1}{2}}$ where s is the standard deviation of the annual accumulation at each stake, during the period 1971–83, and n is the number of years of observation.

This degree of uncertainty is much greater than the measurement errors. As previously mentioned, it mainly

TABLE I. MEAN ANNUAL ACCUMULATION BETWEEN 1971 AND 1983 FOR STAKES LOCATED BEYOND STATION E40

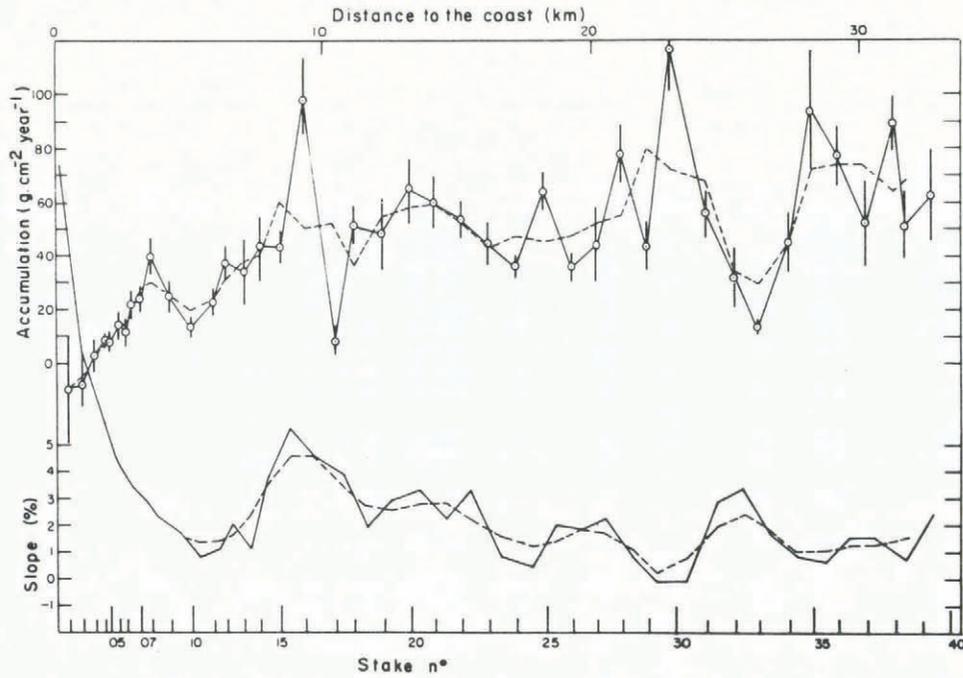| Stake No.	Feb. 1971 to Feb. 1972	Feb. 1972 to Feb. 1973	Feb. 1973 to Feb. 1974	Feb. 1974 to Feb. 1975	Feb. 1975 to Feb.1976	Feb. 1976 to Fen. 1977	Feb. 1977 to Feb. 1978	Feb. 1978 to Feb. 1979	Feb. 1979 to Feb. 1980	Feb. 1980 to Feb. 1981	Feb. 1981 to Feb. 1982	Feb. 1982 to Feb. 1983	Mean value m	Standard deviation s
01	-8				-11								-10	
02	-9		84			12	-11	-11					-8	11
03	9	-2			16	17	10	-8	-5	-4	43	-40	3	23
04	4	-15		14	27	16		1	15	-1	31	3	9	15
-05	4	-21		29	39	13	-4	11	5	3	31	-5	8	17
-05 bis	12	-16		34	49	17	4	-1	9	16	36	8	14	18
-06	14	-19	28		40	14	0	-6	9	11	36	6	11	18
-07	28	-4	50		51	32	9	-2	30	28	48	12	24	19
-08	49	4	64		63	58	17	36	51	38	93	10	40	27
-09	29	1	70		57	49	1	-5	99	-35	60	31	30	39
-10	22	-27	20	19	18	21	1	-13	7	-4	31	13	9	17
-11	31	-17	37	25	22	37	6	16	14	25	40	39	23	17
12	63	2	67	21	59	63	11		71	41	97	19	47	30
13	57	-21	-3	89	35	62	4		35	20	63		34	34
14	56	-20	103	6	58	72	41	50		57		44	44	35
-15	59	1	79	33	44		-1	30	68	40	97	45	47	30
16	127	10	127	98	95	198	70	119		91	71	70	98	47
17		-25	41	8	29	43	-10	-16	8	-13	4	20	8	23
18	90	12	94	66		103	39	25	62	53	53	29	57	30
-19	63	6	66	43	69	78	3	81	51	26	73	27	49	28
20	74	9	87	62		104	30	47	73	55	99		65	31
-21	79	-5	84	59	69	102	28	37	77	45	83	62	60	30
-22	59	-10		114	56	85	3	25	86	26	52	37	44	32
-23	68	-13	129		56	92	11	99	16	21	58	20	46	37
24	36	-11	97		45	67		0	-7	4	14	17	24	26
25	102	13	167		71	119		53	53	65	81	31	69	33
26		-15		126	49	99	28	37	60	62	81	49	52	33
-27	57	6		140	55	85	27	17	17	31	58	36	44	24
28	64	30				121	54	66	86	99	118	64	78	30
29	97	8		154	51	66		19	2	13	47	28	44	31
30					51	154	99	124	104	98	276	61	131	70
31	14			168	52	83	20	32		52	79	66	57	26
32	-2	-8		37	24	42		11	114	57	46		32	39
33	4	-7		104	29		-1	-9	-6	-4	5	27	13	14
34	93	21					35	31	31	47	84	16	45	29
35	10	152					63	55	94	111	197	73	94	59
-36	32	107		90	59	106	66	61	108	81	161	57	77	37
-37	8	-7		110	34	74	23	39	52	100	139	55	52	44
38	9	137		194	76		57	82	91	114	176	56	90	49
39		-8		106	24		30	25	78		131	76	51	47
40		-2				69	82	-5	76	89	143	51	63	49
													43	31

490

Fig. 4. Upper curves: mean values of the annual balance between the coast and stake E40 deduced from stake measurements for the period 1971–83. The 1σ precision is plotted. Lower curves: slope change from one stake to the next. (---) three points running mean.
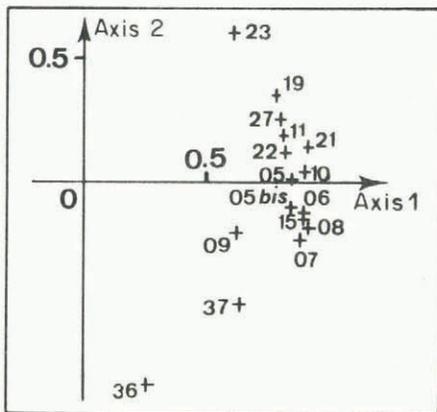

Fig. 5. Principal component analysis of reduced centred fluctuations of annual accumulation. For 10 years and 16 stakes (located between the coast and stake 37).

reflects the temporal variation of accumulation and allows us to compare stations measured at different times.

Between the coast and stake D15 (Fig. 4), we noted a well-marked altitude effect. After D15, this effect becomes secondary relative to major deviations observed from one stake to another. These deviations cannot be directly attributed to variations in relief; between L25 and E40, accumulation increases in the "hollows" and decreases on the "hills"; however, this effect is reversed between stakes D15 and L25.

For this time period, ranging from 1971 to 1982, we computed the annual accumulation in the area from D10 to D21 (Table IV). Comparing these values with mean annual temperatures at Dumont d'Urville (Fig. 6), we can deduce that the local mean annual temperature does not govern this variation in accumulation directly.

From the total set of observations, we conclude that between the coast and stake E40, the spatial variations in accumulation are considerable and cannot readily be
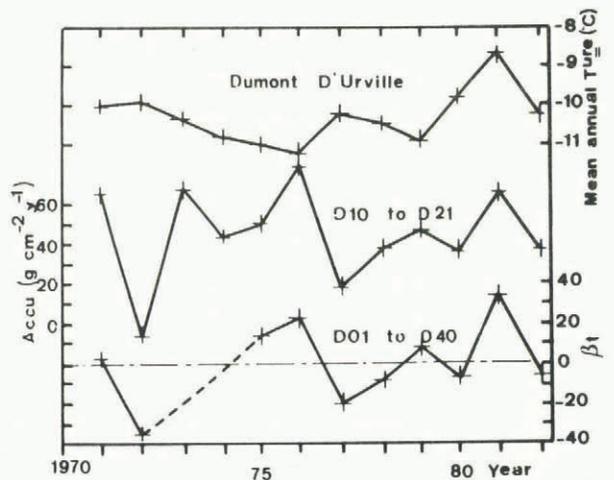
Fig. 6. Mean annual temperature at Dumont d'Urville (upper curve) compared with the mean annual accumulation between: D10 to D21 (middle curve); D01 to D40 (lower curve).

TABLE II. ACCUMULATION MEASUREMENTS AT THE BAMBOO NETWORKS FOR THE YEAR 1972

Stake No.	D9	D50	D59	D80
1		2.7	32.5	46
2	−4	9		15
3	14	27.5	41.3	30.6
4	42	35		26.4
5		30		6.2
6	27	33	29.7	34.5
7	−17	11	35.3	53
8	11.5	41		36.2
9	43	39.5	42	33
$\overline{m}$	16.6	25.4	36.2	31.2
σ	55	40	11	40

TABLE III. TOPOGRAPHIC MEASUREMENTS AND ACCUMULATION RATE DETERMINED BETWEEN STAKE J01 AND STAKE E40

Station	Distance	Altitude	Slope	Number of years	Method	Period	Accumulation ±σ	Reference	10 m temperature
	km	m	%				g cm⁻² year⁻¹		°C
Cap Prudhomme	0	0							
			132						
J01	0.50	66		2	s	1971–77	−10 ± 20		
			73						
D02	1.00			8	s	1971–79	−8 ± 8		
D03	1.45	135		12	s	1971–83	3 ± 6		
L04	1.80		51	11	s	1971–83	9 ± 3		
D05	2.00	163		19	s	1962–83	8 ± 4		
D04bis	2.35		36	12	s	1971–83	14 ± 5		
D06	2.55	183		12	s	1971–83	11 ± 5		
A3			31	12	s	1956–69	22 ± 5	(1)	
D07	3.10	200		12	s	1971–83	24 ± 5		
			25						
D08	3.50	210	19	12	s	1971–83	40 ± 7		
D09(ex.A5)	4.20	223		22	s + β	1955–83	25 ± 6	(2)	
			15						
D10*	5.00	235	17	18	s + β	1965–83	13 ± 4	(2)	−14.4
D11	5.85	241		12	s	1971–83	23 ± 5		
			10						
L12	6.35	246		27	s + β	1955–83	37 ± 6	(3)	−15.3
R13*	7.05	260		10	s	1971–82	34 ± 13		
			10						
M14	7.65	266		8	s	1971–83	44 ± 12		
			37						
D15	8.45	296		17	s + β	1965–82	43 ± 6	This work	−16.2
M16	9.35	346		11	s	1971–83	98 ± 14		
			54						
E17	10.45	396		11	s	1972–83	8 ± 7		
			38						
J18*	11.10	421		18	s + β	1965–83	51 ± 7	This work	−16.5
			18						
D19	12.15	440		12	s	1971–83	49 ± 14		
			29						
J.20	13.20	470		10	s	1971–82	65 ± 10		
			32						
D21	14.15	500		12	s	1971–83	60 ± 9		−17.3
			22						
M22	15.20	523		14	s + β	1969–83	53 ± 7	This work	
			33						
D23	16.20	556		18	s + β	1965–83	44 ± 8	(3)	
			9						
L24*	17.15	565		27	s + β	1955–83	36 ± 4	This work	−17.7
			4						
L25	18.20	569		17	s + β	1965–83	64 ± 7	This work	−17.6
			20						
E26	19.20	589		28	s + β	1955–83	35 ± 5	(3)	−17.9
			19						
D27	20.15	607		12	s	1971–83	44 ± 13		
			22						
J28	21.15	629		9	s	1971–83	78 ± 11		
			9						
L29	22.15	638		11	s	1971–83	44 ± 9		
			−2						
J30	23.15	636		6	s + β	1977–83	117 ± 16	This work	−17.8
			−2						
M31	24.25	634		10	s	1971–83	57 ± 9		
			28						
D32	25.25	662		10	s	1971–82	32 ± 11		
			33						
K33*	26.10	690		27	s + β	1955–83	13 ± 3	(3)	−18.3
			16						
K34	27.30	709		8	s	1971–83	45 ± 11		
			9						
K35	28.20	717		8	s	1971–83	94 ± 22		
			5						
D36	29.20	722		12	s	1971–83	77 ± 11		
			15						
D37	30.20	737		12	s + β	1971–83	52 ± 16	This work	−19.1
			15						
K38	31.20	752		11	s	1971–83	90 ± 10		
			7						
N39	32.20	759		10	s	1971–83	51 ± 13		
			24						
E40*	33.20	783		9	s	1971–83	63 ± 17		−19.5

*Stations positioned by the Doppler-effect survey.
s Accumulation determined by stake measurement.
β Accumulation determined by β radioactivity.

References

1. Lorius and others, 1970.
2. Lambert and others, 1977.
3. Pourchet and others, 1983.

TABLE IV. MEAN ANNUAL TEMPERATURE AT DUMONT D'URVILLE COMPARED TO MEAN ANNUAL ACCUMULATION BETWEEN D10 TO D21

Year	Mean accumulation between D10 and D21 g cm^{-2} year^{-1}	Mean annual temperature at Dumont d'Urville °C
1971	66	−10.0
1972	−6	− 9.9
1973	68	−10.3
1974	44	−10.8
1975	50	−11.0
1976	80	−11.2
1977	18	(−10.2)
1978	38	−10.4
1979	47	−10.9
1980	36	− 9.8
1981	65	− 8.7
1982	37	−10.3

explained by the relief. On the other hand, the temporal variations are quite homogeneous from one stake to another, but these variations are not governed simply by temperatures.

Beyond stake E40

Table V gives all the relevant data available for this area. For each accumulation figure, we give a mean standard deviation (σ) corresponding to the 90% annual variability we measured in the preceding area.

From stake E40 (Fig. 7), a continuous decrease in accumulation (A) is observed when plotted against the distance to the coast. This decrease can be expressed by

$$A = \gamma e^{\omega x}$$

where x is the distance to E40, and γ and ω are two constants. When A is expressed in g cm^{-2} year^{-1} and x in km, we find

$$\gamma = 40.3 \text{ g cm}^{-2} \text{ year}^{-1}$$

$$\omega = -248 \times 10^{-5} \text{ km}^{-1}.$$

Between E40 and R60, large cyclic variations are superimposed on a decreasing mean trend. For this area, the accumulation (Y) can be expressed by the product of two factors: a decreasing (A) governed mainly by temperature and a deviation (B) associated with a wave function that can be expressed:

$$Y = AB.$$

This correcting term (B) is given by

$$B = 1 + \delta \sin(\alpha x + \beta).$$

In our case we find

$$\beta \neq 0,$$

$$\alpha = 120/13 \text{ km}^{-1},$$

$$\delta \neq 0.3.$$

The complete expression of the accumulation between E40 and R60 becomes

$$Y = (40.3 \exp -0.00248x)(1 + 0.3 \sin 120x/13).$$

These periodic oscillations in the accumulation revealed between E40 and R60 cannot be explained by a simple relationship with the relief as seems to be the case in the vicinity of Wilkes Station (Black and Budd, 1964). We suggest a meteorological explanation for this phenomenon.

METEOROLOGICAL ANALYSIS OF OBSERVED ACCUMULATION OSCILLATIONS

Outline of the problem

The above results show that from the point of break in slope of the Antarctic plateau, near stake R60, the accumulation of snow (which is almost uniform on this plateau) changes in a periodic manner with distance, until reaching the coastal area, with a quasi-constant wavelength of about 40 km.

In this area there is no melting of snow. The accumulation of snow therefore represents roughly the annual precipitation. However, the spatial distribution can be non-uniform due to the combined effects of wind and relief, which will now be discussed.

Precipitation conditions

In order to establish the most frequently occurring conditions of precipitation in the Terre Adélie area, we use the data collected during the International Geophysical Year (1957–58). This information is quite old but it is more continuous and better documented than data collected from automatic weather stations installed since the I.G.Y. In particular, the Charcot meteorological weather station (lat. 69°22′ S., long. 139°01′ E., 2400 m elevation) was operational during the I.G.Y. period, next to the break-in-slope location. This location is ideal for an appreciation of the meteorological conditions both on the plateau and at the summit of the slope line.

On the other hand, the climate at the permanent Dumont d'Urville meteorological station is largely influenced by the ocean and by the katabatic winds.

Table VI shows that in winter (April–September) at Charcot, the number of days of blowing snow is always higher than the number of days of snowfall. This confirms the idea that wind plays a major role in spreading the snow accumulation. Furthermore, the number of days of blowing snow at Charcot is higher than at Dumont d'Urville. This strong contrast can be explained by the fact that Dumont d'Urville is influenced by oceanic conditions and that in the case of katabatic wind, the hydraulic jump, physically described as the "blowing-snow wall" (Valtat, 1960), which greatly reduces the strength of the surface wind, often occurs on the slope up-stream of Dumont d'Urville.

Snow transport by wind

The snow is transported by wind, either during precipitation or by uplift from the surface by turbulence. Figure 8 shows the probability of finding snow particles in suspension in the air as a function of wind speed at a height of 10 m (Radok, 1968). In order to define this curve, the author assumed that the mean snowfall speed, in the proximity of the surface, was 0.3 m/s. This value was determined from measurements conducted at Byrd Station (Antarctica) and corresponds well to the type of snow falling on the well studied area. Moreover, these measurements have shown that the average fall speed near the surface is weakly dependent on the horizontal wind strength.

At a wind speed of 5 m/s, 10% of upward currents already exceed the fall speed of the snow. At Charcot, curtains of blowing snow were observed in spite of wind speeds no greater than 5 m/s (Garcia, 1960). If the wind is greater than 20 m/s, 70% of upward currents exceed the fall speed. Table VII shows the mean values of the main meteorological features at Charcot Station in 1958. Over the year, there is a total of 326 days of blowing snow. The monthly mean wind speed is never less than 6.9 m/s. The monthly maximum wind speeds are always greater than or equal to 20 m/s, except in February (15 m/s).

Table VI shows that in 1957 the number of days of blowing snow was less (261). But, even if 1958 was an exceptional year, we can still conclude that deposition of snow occurs mainly under strong wind conditions.

Generally, there are two modes of snow transport by wind (Male, 1980):

TABLE V. OBSERVATIONS AND MEASUREMENTS BETWEEN STAKE E40 AND DOME C

Station	Distance to E40 km	Altitude m	Number of years	Method	Period	Accumulation g cm^{-2} year^{-1}	Reference	10 m temperature °C
D41	9	924	10	s + β	1965–78	60 ± 18	(2)	−19.8
J41	12	965	7	β	1969–76	70 ± 29	(2)	−21.0
D42	18	1028	23	s + β	1955–83	32 ± 6	(3)	
D43	27	1143	21	β	1955–76	24 ± 5	(3)	−22.6
N44	37	1263	5	s	1972–83	30 ± 14		
D45	47	1353	23	s + β	1955–83	42 ± 8	(2)	−24.0
D46	57	1456	8	s	1972–83	56 ± 19		
N47*	68	1524	26	s + β	1955–83	26 ± 5	(3)	−25.8
D48	78	1594	4	s	1972–76	32 ± 17		
D49	88	1659	6	s	1972–83	41 ± 16		
N50	98	1709	25	s + β	1955–83	24 ± 4	(2)	−27.6
D51	108	1769	11	s	1972–83	22 ± 6		
D52*	118	1831	11	s	1972–83	25 ± 7		
D53	128	1898	28	s + β	1955–83	36 ± 6	(3)	−29.8
D54	138	1927	11	s	1972–83	31 ± 9		−29..8
D55N	143	1963	13	β	1965–78	13–20 ± 4	This work	
D55	148	1995	28	s + β	1955–83	8 ± 2	This work	
D55*			28	s + β	1955–83	5 ± 1	(3)	−31.1
D55S	153	2053	13	β	1965–78	16 ± 4	This work	
D56	158	2063	11	s	1972–83	33 ± 9		−31.0
D57N	163	2052	-	-				
D57*	168	2071	18	s + β	1965–83	41 ± 9	This work	−31.6
D57S	173	2120	-	-				
D58	178	2149	4	s	1972–76	29 ± 15		−32.6
D58S	183	2200	26	β	1955–81	4 ± 1	This work	
590	184		5	s	1978–83	14 ± 7		
D59*	188	2228	28	s + β	1955–83	32 ± 5	(2)	−34.3
R60*	201	2291	21	β	1955–76	26 ± 7	(2)	−36.3
D61	211	2299	4	s	1972–76	33 ± 7		
D62	221	2318	4	s	1972–76	27 ± 14		−37.9
D63	231	2316	4	s	1972–76	25 ± 13		
D64	241	2333	4	s	1972–76	21 ± 11		
R65*	251	2334	1	s	1972–73	25 ± 23		
D66	261	2357	18	s + β	1955–73	20 ± 4	(2)	−38.8
D67	272	2372	1	s	1972–73	20 ± 18		
D68	282	2379	1	s	1972–73	19 ± 18		
D69	293	2379	1	s	1972–73	26 ± 23		
R70*	303	2395	1	s	1972–73	15 ± 13		
D71	313	2407	1	s	1972–73	9 ± 8		
D72	324	2412	18	β	1955–73	23 ± 7	(2)	−41.2
D73	334	2408	1	s	1972–73	11 ± 10		
D74	345	2423	1	s	1972–73	15 ± 13		
R75*	355	2436	1	s	1972–73	13 ± 12		
D76	364	2435	1	s	1972–73	18 ± 16		
D77	373	2407	1	s	1972–73	22 ± 20		
D78	382	2477	1	s	1972–73	12 ± 10		
D79	391	2479	1	s	1972–73	16 ± 14		
R80*	399	2487	28	β	1955–83	24 ± 4	This work	−41.4
D100	600		17	β	1955–72	13 ± 3	(2)	−46.3
D120	800		17	β	1955–72	8 ± 2	(2)	−52.3
Dome C	1040	3240	25	β	1955–80	3.2 ± 0.6	(4)	−53.5

*Stations positioned by the Doppler-effect survey.

References

2. Lambert and others, 1977.
3. Pourchet and others, 1983.
4. Petit and others, 1982.

Saltation. Within a 10 cm thick layer above the surface, the snow particles follow a curved trajectory under the influence of gravity and the drag force resulting from the relative speed between the wind and the particles (Fig. 9).

Diffusion. When the wind reaches a certain level, the particles are transported in suspension in the air by turbulent diffusion.

In either case, experience shows that, due to inhomogeneities of the medium and the surface beneath, the travel distance of the particles is low, around a few meters, and that they give rise to low-height undulations on the surface.

Dunes. We assume that dunes are built up in the same way as undulations (Dallavalle, 1948). The heavier particles build up at the top of undulations until they form ridges and then dunes when the wind frequently blows in the same direction. The undulation wavelength depends on the wind strength and increases together with their crest height.

Effect of relief. The effect of relief on the accumulation of snow has not been studied for the relevant scale (about 50 km in horizontal distance). On a small scale (small hills or buildings), snow is known to deposit on the wind-protected side (Radok, 1977).

However, Figure 10 (Dallavalle, 1948) demonstrates that in the dune travel mechanism, the particles accumulate on the exposed side instead of in the hollows between undulations.

Thus, hills do not fill in but move instead, very slowly, in the direction opposite to that of the prevailing wind.

Experimental remarks. In the area of interest, there is a strong correlation between the isotope content of the snow and the mean annual temperature of the related location (Lorius and Merlivat, 1977). The isotope content varies linearly with the distance from the coast. These observations are incompatible with snow transport by wind, heterogeneous by nature, over long distances (exceeding 10 km).
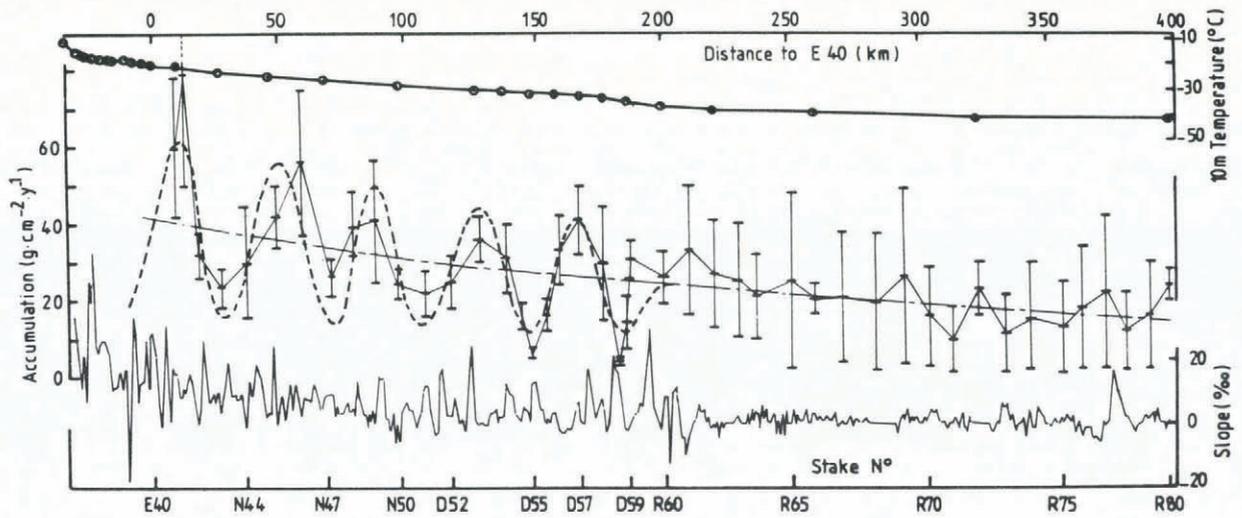
Fig. 7. *Variations of three parameters along the Dumont d'Urville–R80 axis. Upper curve: 10 m depth snow temperature. Middle curve: accumulation measurement for the longest period observed. ⎯⎯ Individual measurement. Accumulation explained by temperature variations. --- Accumulation explained by temperature variations and wave function. The 1σ uncertainties associated with individual measurements are given by the number of years of observation. Lower curve: 1 km mean slope along the Dumont d'Urville–R80 axis.*

TABLE VI.   NUMBER OF DAYS OF SNOWFALL AND SNOW-BLOW AT DUMONT D'URVILLE AND CHARCOT DURING THE INTERNATIONAL GEOPHYSICAL YEAR (1957–58) (AFTER CORNET AND OTHERS, 1960)

Dumont d'Urville		J	F	M	A	M	J	J	A	S	O	N	D	Total
Snowfall	1957	13	10	12	12	8	10	11	9	9	8	14	8	124
	1958	15	9	18	12	4	5	12	15	8	11	7	8	124
Snow-blow	1957	1	5	9	18	12	15	18	15	16	15	6	1	131
	1958	6	4	19	14	6	10	11	19	15	11	7	6	128
Charcot														
Snowfall	1957	x	x	3	3	3	0	2	3	2	2	5	5	28
	1958	8	4	12	10	8	4	15	15	1	7	4	8	96*
Snow-blow	1957	x	x	20	28	25	30	27	28	28	29	27	19	261
	1958	25	24	30	29	29	30	28	28	30	29	23	21	326†

* 84 from March to December.
† 271 from March to December.

A comparison of the curves in Figure 7 shows that snow accumulation and the slope of the surface, as a function of distance from the coast, are not correlated.

We observe a strong contrast between the plateau, where accumulation is relatively uniform and slopes are shallow, and the slope area, where accumulation takes on a cyclic mode and slopes are steep.

Conclusion. These last three observations allow us to conclude that the mechanisms described previously can explain undulation formation with a wavelength up to about 10 km.

However, the redistribution of snow by wind in such a way cannot occur on a sufficient scale to explain the cyclic mode of snow accumulation with a wavelength of 40 km.

We must therefore seek a large-scale atmospheric phenomenon causing the modification of snow deposition. Such a phenomenon could be an atmospheric wave inducing "lift-up" or "fall-down" areas. These two distinct areas could locally inhibit or enhance snowfall, which would then be deposited in a non-uniform manner on the surface.

However, each system must respect certain special conditions: the wind must have an almost uniform direction and be of sufficient strength; the atmospheric wavelength must be almost constant and the disturbance must be triggered by the "break in slope".
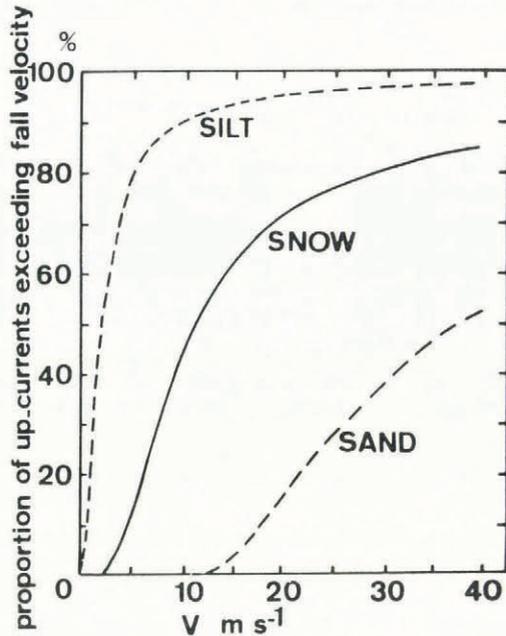
495

Fig. 8. Cumulative frequency curves of suspension up-currents for silt, snow, and sand (after Radok, 1968).
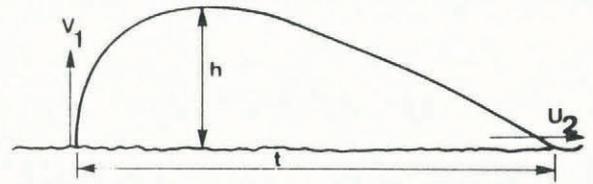

Fig. 9. Trajectory of a particle during saltation (after Male, 1980).

the direction of the slope. Over the cold air layer is warmer air separated from the former by a fluid interface, and generated in the atmosphere by a thin temperature inversion layer.

This type of flow can be studied using the two-layer model proposed by Ball (1956). However, because of the horizontal scale involved (in the order of 100 km) and the proximity of the South Pole, we cannot neglect Coriolis force effects. Once again, based on a two-layer model, the effects of the Coriolis force have been studied by Ball (1960) and by Gutman and Khain (1975).

In the following sections, we shall follow these works but restrict ourselves to the study of the conditions of formation of gravity–inertia waves in the area of interest.

Equations. We choose the case causing the flow of two fluids of different densities superimposed and separated by an interface (Fig. 11). ρ_0 is the density of the upper fluid, ρ_1 is that of the lower fluid, h is the height of the interface measured up from the surface, and δ is the height relative to the x–y plane.

The Y-axis is perpendicular to the plane of Figure 11. We assume that the problem can be reduced to two dimensions by invariance perpendicular to the x–z plane.

At elevation H in the upper fluid, the atmospheric

Determination of the system of equations

The aim is to establish a system of equations relative to the given problem allowing us to study the conditions for the formation of a gravity–inertia wave.

Antarctic climatology shows that, due to temperature differences between the continent and the sea, an eastward circulation prevails in the low troposphere, from the surface up to 3000 m (Alt, 1960).

Resulting from this, and in the area of interest, the winds mainly show a constant direction, satisfying one of the wind conditions and reducing the problem to two dimensions.

Observations show that katabatic winds are very frequent in this area (Valtat and others, 1960).

We can therefore assume that the second condition, strong winds, will generally be satisfied. A katabatic wind is induced by a cold (dense) air flow, caused by gravity in
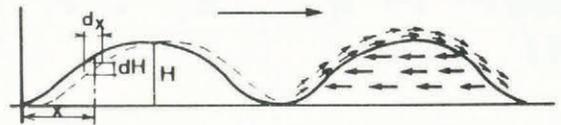

Fig. 10. Schematic illustration of dune travel (after Dallavalle, 1948).

TABLE VII. METEOROLOGICAL DATA DURING THE INTERNATIONAL GEOPHYSICAL YEAR (1957–58) AT CHARCOT (lat. 69°22′ S., long. 139°01′ E., 2400 m altitude)

|	Jan.	Feb.	Mar.	Apr.	May	Jun.	Jul.	Aug.	Sept.	Oct.	Nov.	Dec.	Year
Mean temperature (°C)	−22.1	−30.6	−34.4	−38.5	−41.4	−49.8	−41.7	−43.2	−51.6	−30.7	−30.5	−23.7	−37.3
Minimum	−31.0	−44.2	−43.8	−55.2	−54.9	−61.5	−61.5	−60.2	−61.5	−55.7	−42.0	−33.5	−51.1
Maximum	−10.7	−20.4	−15.0	−21.0	−14.0	−27.0	−17.6	−19.6	−40.9	−16.9	−20.3	−17.1	−21.5
Mean pressure (1/10 mbar)	730.0	726.3	225.3	724.7	728.4	713.2	725.5	715.5	706.9	715.9	721.1	724.2	721.1
Minimum	718.5	717.6		713.7	707.3		698.4	697.4	692.9	695.5	744.5	713.0	705.0
Maximum	743.2	734.6	710.5	739.6	752.3	738.5	741.6	735.6	725.2	733.0	731.9	734.7	735.5
Relative humidity (%)		65	73	75	75	73	75	76	72	71	66	68	71
Average wind speed (m/s)	9.4	8.9	10.8	10.9	8.0	11.9	8.4	8.1	10.5	8.7	7.8	6.9	9.2
Maximum	24	15	26	26	20	29	23	27	26	21	20	26	23.8
Prevailing direction	150°	180°	160°	160°	170°	170°	200°	170°	170°	170°	155°	150°	170°
Mean 700 mbar elevation	2710	2671	2632	2643	2674	2527	2645	2555	2169	2559	2615	2651	2614
Snow-blow days	25	24	20	29	29	30	28	28	30	29	23	21	326
Fog		13	24	30	25	29	25	25	30	18	10	10	239
Snow	8	4	12	10	8	4	15	15	1	7	4	8	96
Rime	1	0	1	3	4	2	4	2	0	0	4	0	21
Aurora	0	0	0	1	5	0	6	5	1	0	0	0	18
Ice crystals	0	0	0	0	0	0	1	2	1	2	0	0	6
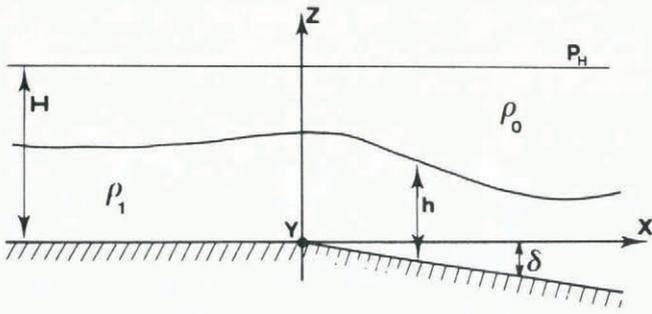
Fig. 11. *Air flow beneath an inversion layer. The base of the inversion is idealized as an interface between two fluids of different densities ρ_0 and ρ_1.*

pressure is P_H and we assume that geostrophic equilibrium is established, expressed as:

$$v_g = -\frac{1}{\rho_0} f \frac{\partial P_H}{\partial y} = \text{constant},$$

$$v_g = -\frac{1}{\rho_0} f \frac{\partial P_H}{\partial x} = \text{constant}. \tag{1}$$

The hydrostatic equation allows us to express the pressure P_1 in the lower layer, at a height Z, as

$$P_1 = P_H + \rho_0 g H + (\rho_1 - \rho_0)g(h + \delta) - \rho_1 g z. \tag{2}$$

The standing-wave equations can be written

$$u\frac{du}{dx} = -\frac{\rho_1 - \rho_0}{\rho_1} g \, d\frac{h + \delta}{dx} + f(v - V_g)$$

$$u\frac{dv}{dx} = f(V_g - u) \tag{3}$$

$$\frac{du}{dx}h = 0$$

where f is the Coriolis parameter, u and v are the horizontal components of the speed respectively in directions x and y. We can write the expressed variables in a dimensionless form by introducing a critical speed $U_c = (g' Q)^{1/3}$ where $Q = Uh = \text{constant}$ and

$$g' = \frac{\rho_1 - \rho_0}{\rho_0} = \frac{\Delta\theta}{\theta} g$$

where $\Delta\theta$ is the potential temperature difference between the cold air layer of temperature θ which flows down the slope and the warmer air which is on top.

The dimensionless variables, with a bar over them, are expressed by

$$x = \frac{U_c}{f}\bar{x}; \quad u = U_g\bar{u}; \quad v = V_g = U_c\bar{y}$$

and

$$z = \frac{U_c^2}{g'}\bar{z}.$$

Then the system of Equations (3) is written in dimensionless form, omitting the bars:

$$\alpha u\frac{du}{dx} + \frac{dh}{dx} + \frac{d\delta}{dx} = v$$

$$u\frac{dv}{dx} = 1 - u \tag{4}$$

$$uh = 1$$

where

$$\alpha = \left[\frac{U_g}{U_c}\right]^2$$

is the dimensionless parameter for the problem which depends on a Froude number. In fact,

$$\alpha^{3/2} = \frac{U_g}{u} F^2 \quad \text{where} \quad F = \frac{U_g}{\sqrt{g' h}}.$$

The relief is expressed in a simple way in accordance with Figure 11.

$$x < 0 \qquad \delta = 0$$

$$x > 0 \qquad \delta = kx.$$

In the system of Equations (4), h can be eliminated, and the system becomes, for $x > 0$:

$$\alpha u\frac{du}{dx} - \frac{1}{u^2}\frac{du}{dx} + k = v$$

$$u\frac{dv}{dx} = 1 - u. \tag{5}$$

This system in Equations (5) can be integrated:

$$v = k \pm \left[\left[\frac{1-u}{u}\right]^2 (1 - \alpha u^2) + C\right]^{1/2} \tag{6}$$

where C is an integration constant.

We are looking for the periodic behavior of the vertical component of speed W. Based on the assumption made earlier, W can be written, for $z = h$, as
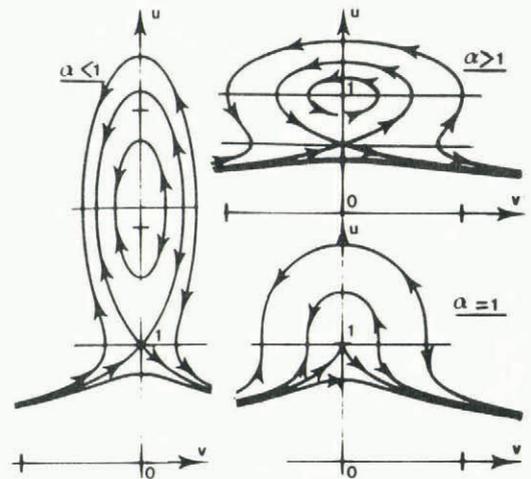
$$W = u\frac{dh}{dx}.$$

Fig. 12. *Schematic representation of possible phase-plan variants.*

497

Because of the continuity equation of system (3), we can express W as

$$W = -h \frac{du}{dx}.$$

The du/dx expression we could obtain, using Equations (5) and (6), would be too complicated to demonstrate easily its periodic behavior along the x-axis. However, we know that if u shows a periodic behavior along the x-axis, then the same holds for du/dx and consequently for W.

We can study graphically the behavior of u and v deduced from Equation (6). Three cases are to be considered:

$$\alpha < 1, \quad \alpha = 1, \quad \text{and} \quad \alpha > 1 \qquad \text{(Fig. 12)}.$$

The curves are drawn with $k = 0$. Curves corresponding to different values of k may be obtained by a translation on the v-axis.

The arrows show the movement for increasing values of x, and are obtained by studying the sign of the following equations:

$$du = v \frac{u^2}{\alpha u^3 - 1} dx$$

$$\tag{7}$$

$$dv = \left[\frac{1}{u} - 1 \right] dx.$$

The case where $\alpha > 1$ is the only one giving a closed curve with a continuous movement, i.e. with the arrows always in the same direction.

In this case, where $\alpha > 1$, u and v vary periodically along the x-axis, around an equilibrium point $u = 1$ and $v = 0$. In the following sections, we only consider this case, excluding the others.

Wavelength. Figure 13 shows the graphical solution of Equation (6) for the case of $\alpha > 1$ and $k < 0$.

When $x < 0$, there is an unique solution: $u = 1$ and $V = 0$, designated as point a, which corresponds to geostrophic balance. For $x = 0$, as $|k|$ increases, we obtain ellipses increasing in size and centred around the point $v = k$ and $u = 1$, corresponding to different waves as long as the curve is closed.
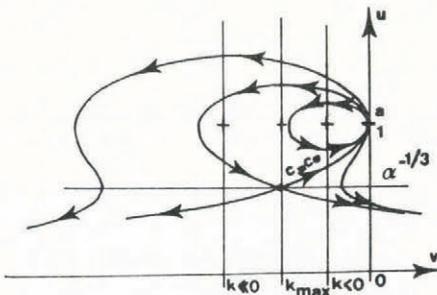

Fig. 13. Schematic representation of phase-plan integral curves used to construct the wave solution of the problem ($\alpha > 1$).

The maximum value of the periodic solution is reached when the solution crosses a singular point: $v = k_{max}$ and $u = \alpha^{-1/3}$, which corresponds to a value of the integration constant:

$$c = c_0 = (\alpha^{1/3} - 1)^3.$$

If $|k|$ is greater than $|k_{max}| = c_0^{1/2} = (\alpha^{1/3} - 1)^{3/2}$, the curve is not closed and there is no periodic solution.

In this case, the maximum amplitude of the wave is obtained for $v = k$, $u = \alpha^{-1/3}$. Then we can integrate Equations (7) between the two values where $v = k$, and we obtain the wavelength:

$$\lambda_0 = 2 \int_{\alpha^{-1/3}}^{(1 - \alpha^{-1/3}) + \left[1 - \alpha^{-1/3}(1 - \alpha^{-1/3})\right]^{1/2}} \frac{\alpha^{2/3} u^2 + \alpha^{1/3} u + 1}{u \left[1 + 2(\alpha^{1/3} - 1)u - \alpha^{1/3} u^2\right]^{1/2}} du. \tag{8}$$

Otherwise, we can assume that the amplitude of oscillation is small and that we remain near geostrophic equilibrium. In this case, the graphical solution is a small ellipse centred at the point: $v = 0$, $u = 1$.

A simple analytical solution can be obtained by linearization of the system of Equations (7), which becomes

$$(\alpha - 1) du/dx = v$$
$$\tag{9}$$
$$dv/dx = 1 - u.$$

v can be removed from these two equations, giving

$$(\alpha - 1) d^2u/dx^2 = 1 - u.$$

We write $u - 1 = A \cos (2\pi/\overline{\lambda_0})x$, where A is a constant and $\overline{\lambda_0}$ is the λ_0 dimensionless wavelength

$$\overline{\lambda_0} = 2\pi(\alpha - 1)^{1/2}. \tag{10}$$

Return to dimensional values and discussion. To explain the cyclic variation of the accumulation of snow along a slope by an atmospheric wave, the atmospheric wavelength λ_0 must be of the same order of magnitude as the wavelength of accumulation observed at the surface, i.e. $\lambda_0 = 4 \times 10^4$ m. Ball (1960) has shown that the wavelengths for the low-amplitude solution (Equation (10)) and for the long-amplitude solution (Equation (8)) are very close to each other.

So we can write the dimensional wavelength

$$\lambda_0 = 2\pi \frac{U_c}{f}(\alpha - 1)^{1/2}$$

with f being the Coriolis parameter: $f = 1.4 \times 10^{-4}$ s^{-1}. This gives

$$(\alpha - 1)^{1/2} = \frac{2.8}{\pi U_c} \quad \text{where} \quad U_c = (g' U_h)^{1/3}.$$

In the expression of U_c, g' and h are well known.

Observations (Valtat and others, 1960) show that we can expect temperature gradients from 5K up to 10K between the cold air layer and the warmer air on top. In this case, for a mean cold-air temperature of 250K, g' varies from 0.2 to 0.4 m s^{-2}. The thickness of the cold air layer usually varies from 500 to 1000 m. U, however, is not known. It is the mean speed of the cold air which flows down the slope due to gravity in a uniform and steady manner (Ball, 1956). For U, let us take a very low value of 1 m s^{-1} together with the lowest values for g' (0.2) and for h (500 m). In this case, $U_c = 4.64$ m s^{-1}.

Considering these assumptions, we obtain a maximum value of α

$$\alpha = 1 + (2.8/4.64\pi)^2,$$

$$\alpha = 1 + 0.04.$$

α must satisfy the $\alpha > 1$ condition, and nevertheless remains at a value around 1.

This result excludes the exact maximum-amplitude solution (Equation (8)). Indeed, we respect the condition:

$$|k| < (\alpha^{1/3} - 1)^{3/2}$$

but

$$|k| = \frac{\bar{z}}{\bar{x}} = \frac{g'}{U_C f} \left|\frac{z}{x}\right|.$$

Since the relief drops about 2000 m over 200 km, we have

$$\left|\frac{z}{x}\right| \simeq 10^{-2}.$$

Furthermore, since α must be about 1, U_C is required to be of the same order of magnitude as U_g. If we choose a high value of U_C (30 m s^{-1}) and a low value of g' (0.2), so that $|k|$ must be small, we find:

$$|k| \simeq 0.95; \text{ this value leads to}$$

$$\alpha = [(0.95)^{2/3} + 1]^3 = 7.62.$$

We conclude that the only possible solution is the one corresponding to a disturbance occurring near geostrophic equilibrium and satisfying the system of Equations (9).

However, we must verify that α can be equal to 1 and that it stays near this value.

We have seen that α can be written as the product of two Froude numbers:

$$\alpha = FgFu^{-1/3}$$

where $Fg = u_g/(g'h)^{1/2}$ is a Froude number induced by the geostrophic wind and $Fu = u/(g'h)^{1/2}$ is a Froude number induced by the uniform speed of the flow. Ball (1956) has shown that this Froude number depends only on the relationship $Fu = k/C_D$ where k is the slope of the field and C_D is a viscosity coefficient, depending on the surface structure.

So, although U and h can vary along the slope (we generally admit that g' variation is low), the Froude number Fu of uniform flow remains constant.

We know that $k = 10^{-2}$ but C_D is unknown for the study location. However, Ball (1956) obtained C_D values ranging from 10^{-2} down to 5×10^{-3}, so Fu therefore changes from 1 to 2 and the condition $\alpha \simeq 1$ therefore implies that:

$$Fg = Fu^{1/3}.$$

Fg values will range between $Fg = 1$ and $Fg = 1.26$. These values will easily be reached, since the selection of relatively large values for g' (0.4 m s^{-1}) and h (1000 m) gives $Fg = 1.26$ if $U_g = 25.2$ m s^{-1}, which is very reasonable considering the mean wind speed observed in Terre Adélie.

Finally, we note that the order of magnitude of values given by observations for the variables giving the Froude number (geostrophic wind, modified gravity, and layer thickness) lead to $Fg \simeq 1$.

This Froude number represents flow occurring in an area showing marked regularity: uniform surface slope over a long distance; very homogeneous nature and temperature of the surface; atmospheric circulation induced by a slowly changing temperature gradient (continent to sea); stable cold air.

Unfortunately, we presently have insufficient data from lower-layer soundings to confirm this hypothesis.

It can be concluded that a gravity–inertia wave disturbing the geostrophic equilibrium may be formed. Its amplitude is weak but the triggering occurs at the break-in-slope location and the wavelength is of the same order of magnitude as the accumulation wavelength. The conditions for formation of this wave are strictly local in character.

If such an atmospheric wave originates the cyclic behavior of the snow accumulation along the slope in Terre Adélie, we must emphasize that it is a very special case which is unlikely to occur other than in Antarctica.

CONCLUSION

The dating of the snow layers or, in other words, the accumulation is an important parameter for the geochronological studies carried out on the ice cores. As important spatial and temporal variations in the accumulation exist in Antarctica, it is necessary to compare the results for different points to be able to normalize these measurements. Thus, by comparing the accumulation at two different sites, it is possible to measure this accumulation at the same time. On the other hand, by taking into account the scatter of the results due to variations with time, these temporal variations are in general much more important than experimental error. Our work shows that, for an important zone, this normalization must be possible. In fact, more than 50% of the observed variations are not random.

The measurements carried out in the field with bamboo networks showed that the choice of a better reference area for the accumulation measurements should considerably reduce the noise due to sastrugi.

Finally, we suggest a plausible meteorological explanation for the spatial oscillations observed on a part of the measuring axis. For this zone, a parameterization of this phenomenon allows us to diminish the discrepancy between the measured and calculated accumulation in a significant manner.

REFERENCES

Alt, J. 1960. Quelques considérations générales sur la météorologie de l'Antarctique. *Météorologie*, Sér. IV, No. 57, p. 17–39.

Ball, F.K. 1956. The theory of strong katabatic winds. *Australian Journal of Physics*, Vol. 9, No. 3, p. 373–86.

Ball, F.K. 1960. Finite tidal waves propagated without change of shape. *Journal of Fluid Mechanics*, Vol. 9, p. 506.

Black, H.P., *and* Budd, W. 1964. Accumulation in the region of Wilkes, Wilkes Land, Antarctica. *Journal of Glaciology*, Vol. 5, No. 37, p. 3–15.

Cornet, A., *and others.* 1960. Accumulation de neige en Terre Adélie, by A. Cornet, C. Lorius, and G. Ricou. *Météorologie*, Sér. IV, No. 57, p. 175.

Crozaz, G. 1969. Fission products in Antarctic snow, an additional reference level in January 1965. *Earth and Planetary Science Letters*, Vol. 6, No. 1, p. 6–8.

Dallavalle, J.M. 1948. *Micrometrics: the technology of fine particles. Second edition.* Pitman Publishing Corporation, p. 411–15.

Garcia, R. 1960. Mesures du transport de neige par le vent à la Station Charcot. *Météorologie*, Sér. IV, No. 57, p. 205–12.

Gutman, L.N., *and* Khain, A.P. 1975. Mesometeorological processes in the free atmosphere governed by orography. English edition of *Izvestiya, Academy of Sciences, USSR, Atmospheric and Oceanic Physics*, Vol. 11, No. 2, p. 107–17.

Lambert, G., *and others.* 1977. Accumulation of snow and radioactive debris in Antarctica: a possible refined radiochronology beyond reference levels, by G. Lambert, B. Ardouin, J. Sanak, C. Lorius, and M. Pourchet. [*Union Géodésique et Géophysique Internationale. Association Internationale des Sciences Hydrologiques. Commission des Neiges et Glaces.*] *Symposium. Isotopes et impuretés dans les neiges et glaces. Actes du colloque de Grenoble, août/septembre 1975*, p. 146–58. (IAHS–AISH Publication No. 118.)

Llliboutry, L. 1974. Multivariate statistical analysis of glacier annual balances. *Journal of Glaciology*, Vol. 13, No. 69, p. 371–92.

Lorius, C., *and* Merlivat, L. 1977. Distribution of mean surface stable isotopes in East Antarctica: observed changes with depth in the coastal area. [*Union Géodésique et Géophysique Internationale. Association Internationale des Sciences Hydrologiques. Commission des Neiges et Glaces.*] *Symposium. Isotopes et impuretés dans les neiges et glaces. Actes du colloque de Grenoble, août/septembre 1975*, p. 127-37. (IAHS–AISH Publication No. 118.)

Lorius, C., *and others*. 1970. Dating of firn layers in Antarctica: application to the determination of the rate of snow accumulation, by C. Lorius [and 8 others]. [*Union Géodésique et Géophysique Internationale. Association Internationale d'Hydrologie Scientifique.*] [*International Council of Scientific Unions. Scientific Committee on Antarctic Research. International Association of Scientific Hydrology. Commission of Snow and Ice.*] *International Symposium on Antarctic Glaciological Exploration (ISAGE), Hanover, New Hampshire, U.S.A., 3–7 September 1968*, p. 3-15. [(Publication No. 86 de l'Association Internationale d'Hydrologie Scientifique.)]

Male, D.H. 1980. The seasonal snowcover. (*In* Colbeck, S.G., *ed. Dynamics of snow and ice masses.* New York, Academic Press, p. 305-95.)

Petit, J.R., *and others*. 1982. A detailed study of snow accumulation and stable isotope content in Dome C (Antarctica), by J.R. Petit, J. Jouzel, M. Pourchet, and L. Merlivat. *Journal of Geophysical Research*, Vol. 87, No. C6, p. 4301-08.

Picciotto, E., *and* Wilgain, S. 1963. Fission products in Antarctic snow, a reference level for measuring accumulation. *Journal of Geophysical Research*, Vol. 68, No. 21, p. 5965-72.

Picciotto, E., *and others*. 1964. Rate of accumulation of snow at the South Pole as determined by radioactive measurements, by E. Picciotto, G. Crozaz, and W. de Breuck. *Nature*, Vol. 203, No. 4943, p. 393-94.

Pourchet, M., *and others*. 1983. Some meteorological applications of radioactive fallout measurements in Antarctic snows, by M. Pourchet, F. Pinglot, and C. Lorius. *Journal of Geophysical Research*, Vol. 88, No. C10, p. 6013-20.

Radok, U. 1968. Deposition and erosion of snow by the wind. *CRREL Research Report* 230.

Radok, U. 1977. Snow drift. *Journal of Glaciology*, Vol. 19, No. 81, p. 123-139.

Reynaud, L., *and others*. 1984. Spatio temporal distribution of the glacial mass balance in the Alpine, Scandinavian and Tien Shan areas, by L. Reynaud, M. Vallon, S. Martin, and A. Letreguilly. *Geografiska Annaler*, Vol. 66A, No. 3, p. 239-47.

Valtat, B. 1960. Note sur les modifications de structure thermique des basses couches pour divers régimes de vent au sol à Dumont-d'Urville. *Météorologie*, Sér. IV, No. 57, p. 127-33.

Valtat, B., *and others*. 1960. Le "phénomène de Loewe" en Terre Adélie, by B. Valtat, J. Gilbert, and R. Magniez. *Météorologie*, Sér. IV, No. 57, p. 77-112.

MS. received 2 October 1985 and in revised form 28 May 1986